

Efficacy of Polymeric Coatings to Protect Concrete from Physical Salt Attack

M. A. Abuzeid¹, M. R. Sakr², M. T. Bassuoni^{1*}

¹Department of Civil Engineering, University of Manitoba, Winnipeg, Manitoba, R3T5V6, Canada
abuzeidm@myumanitoba.ca; *mohamed.bassuoni@umanitoba.ca (corresponding author)

²Department of Civil Engineering, Faculty of Engineering at Shoubra, Benha University, Cairo, 11629 Egypt
mohamed.ramadan@feng.bu.edu.eg

Abstract - Physical salt attack (PSA) is a deterioration mechanism that is associated with concrete elements subjected to cyclic ambient conditions (i.e., temperature and relative humidity). In this study, two polymeric coatings (ethyl silicate and high-molecular-weight methacrylate) were investigated for their effectiveness to protect three high porosity concrete mixtures, representing the common case for residential concrete in North America, against cyclic conditions stimulating PSA. Visual assessment and mass loss of concrete specimens were used as physical indicators for qualitative and quantitative damage assessments. In addition, thermal and microstructural analyses were conducted to elucidate the deterioration mechanism. Results showed that using high replacement ratios of fly ash and slag caused an inferior resistance against PSA. Ethyl silicate provided superior protection regardless of the mixture type, whereas concrete coated with high-molecular-weight methacrylate experienced severe damage under these harsh conditions.

Keywords: *Physical salt attack, Surface coatings, Repair, Durability, Concrete, Sulfate attack.*

1. Introduction

Physical salt attack (PSA) is a common damage mechanism in partially embedded concrete elements in salt-rich environments (e.g., piles, basement walls, piers, and abutments). PSA occurs within concrete experiencing a continuous supply of salt solution and simultaneous evaporation through the surface layer [1], leading to salt crystallization pressure (estimated at 20 MPa [2]) in near-surface pores [3]. PSA damage is typically manifested as surface scaling and spalling similar in appearance to freezing/thawing damage, with no or limited chemical interaction occurring between the salt brine and hydration compounds [4]. Historically, PSA was confused with the chemical form of sulfate attack, which led to later recognition of PSA as a distinctive damage mechanism of concrete [5, 6]. Thus, focused research has been recently directed towards the protection of concrete exposed to PSA [7-11].

This study assesses the performance of two commercially available surface coatings as a potential protection strategy for concrete exposed to severe conditions of PSA. Ethyl silicate (ES) and high-molecular-weight methacrylate (HMMA) were selected for coating; each performs different function; ES acts as a pore blocker and hydrophobic agent while HMMA is a surface coating that develops as a membrane on surface to prevent aggressive substances from penetrating into concrete [12, 13]. Three base mixtures were selected to represent low-quality concrete which is typically used for residential construction in North America (worst case scenario). Two mixtures incorporated high dosage of supplementary cementitious materials as measure to produce sustainable concrete with lower contribution to the carbon footprint. The performance of such coated mixtures against PSA has not been evaluated in literature.

2. Research Significance

PSA is a key deterioration mechanism for concrete exposed to salt solutions and cyclic environments; therefore, continuous research is still required to enhance the existing findings regarding the protection of concrete under PSA conditions. This study tests two kinds of surface coatings performing different functions as a measure for concrete protection against PSA. Mixtures with high content of fly ash (40%) and slag (60%) were also tested. The results of this study should contribute additional data to the existing body of knowledge on PSA in terms of protection strategies.

3. Experimental Program

3.1. Materials

3.1.1. Concrete mixtures

Three concrete mixtures were selected as base substrates for application of coatings. The water-to-binder ratio (w/b) was 0.60 representing the case of residential concrete (worst case scenario). General use cement (GU), Class F fly ash (FA) and Grade 100 slag (SG), meeting the specifications of CAN/CSA-A3001 [14], were used to prepare single and binary binders at a fixed binder content of 400 kg/m³. Fly ash and slag were incorporated at dosages of 40% and 60%, respectively. **Table 1** presents the physical and chemical characteristics of the used binders. For the coarse aggregate, local natural gravel, with a maximum size of 9.5 mm, a specific gravity of 2.65, and absorption of 2% was used. Fine aggregate was well-graded river sand with a specific gravity, fineness modulus and absorption of 2.53, 2.9, and 1.5%, respectively. **Table 2** shows the proportions of mixtures along with the resulting compressive strengths according to ASTM C39/C39M [15]. Three cylinders (75×150 mm) from each matrix/coating were cast as per ASTM C192/C192M [16], demolded after 24 hours, and then cured for a 56-day period in a standard curing room (22 ± 2°C and relative humidity [RH] >95%) as recommended by CSA A23.1/A23.2 [17] to permit extended pozzolanic reactivity of concrete prepared with supplementary cementitious materials.

Table 1. Chemical composition and physical properties of binder constituents.

	GU Cement	Fly Ash (FA)	Slag (SG)
Chemical composition			
SiO ₂ (%)	19.2	56.0	33.4
Al ₂ O ₃ (%)	5.0	23.1	13.4
Fe ₂ O ₃ (%)	2.33	3.6	0.76
CaO (%)	63.2	10.8	42.2
MgO (%)	3.3	1.1	5.3
SO ₃ (%)	3.0	0.2	2.4
Na ₂ O _{eq.} (%)	0.12	3.2	0.3
Physical properties			
Mean particle size, μm	13.15	16.56	14.12
Specific gravity	3.15	2.12	2.87
Fineness, m ² /kg	390	290	492

Table 2. Proportions of concrete mixtures per cubic meter.

Mixture ID	Cement (kg)	Fly Ash (kg)	Slag (kg)	Water (kg)	Coarse Aggregate (kg)	Fine Aggregate (kg)	56-day Compressive Strength* (MPa)
GU	400	-	-	240	1200	410	35.3 [1.53]
FA	240	160	-	240	1200	346	32.8 [1.37]
SG	160	-	240	240	1200	391	31.4 [1.45]

*Values between brackets are the standard deviations for compressive strength results

3.1.2. Coatings

Two commercially available coatings were selected from different functional categories: ethyl silicate which acts as a water-repellent and pore blocker agent due to its ability to penetrate and react with the hydrated paste, resulting in pore lining/blocking compounds performing these functions [12], and high-molecular-weight methacrylate which fills surface cracks and forms a superficial membrane after setting, preventing penetration of deleterious materials into concrete [13].

3.2. Application Method

After curing, specimens were air-dried for 48 hours at laboratory conditions (20 ± 2 °C and 50 ± 5% RH) and then, each coating was applied according to manufacturers' recommendations on triplicate samples from each mixture. The bottom surface and the lower 2-cm of all specimens were left uncoated to allow for salt solution uptake, simulating partially embedded elements in salt-rich environments. ES was applied using a low-pressure sprayer in two cycles (60 minutes apart)

with each cycle consisting of three successive saturating applications at time intervals of 15 minutes. For HMMA, the resin was well-stirred with a homogenizer for one minute followed by addition of an initiator and mixing for another two minutes. HMMA was then applied to concrete surface using a low-pressure sprayer in two layers separated at 16 hours. All treated specimens were air-dried for 72 hours followed by moist curing for seven days to provide suitable time for any potential interaction between the coatings and concrete surface.

3.3. Testing Program

Absorption and desorption tests were performed to examine the effect of each treatment application on the fluids transport (intake and evaporation) into concrete compared to the reference (uncoated) samples. The test procedures proposed by Sakr et al. [10] were applied on duplicate discs (75×50 mm), and the absorption or desorption percentages at a certain time after 48 hours were calculated according to **Equation 1**, where m_0 is the initial mass of the disc, and m_{48} is its mass after 48 hours.

$$\text{Absorption/desorption (\%)} = (m_0 - m_{48}) / m_0 \times 100 \quad \text{Eq. 1}$$

Coated specimens were air-dried for 48 hours after curing, and their initial masses were recorded. All specimens were then subjected to the accelerated PSA testing conditions proposed by Bassuoni and Rahman [7] since this exposure provided reliable trends concerning the resistance of concrete to PSA within 120 days. One-third of specimens was partially submerged in 10% Na₂SO₄ solution, while the upper drying portion (100 mm) was subjected to cyclic ambient conditions for 120 cycles. Each cycle (24 hours) consisted of two sequential stages: hot/dry stage (40°C ± 2°C and 35% ± 5% RH) for 8 hours and wet/humid stage (20°C ± 2°C and 90% ± 5% RH) for 16 hours. Solution was frequently replenished to maintain its level and fresh solution was used every 30 days. Every 30 cycles, the mass loss of specimens was calculated according to **Equation 2**, where t is the time, m_i is the initial mass of the uncoated or coated cylinder; m_t is the mass of the cylinder at time t .

$$\text{Mass Loss at (t) \%} = (m_i - m_t) / m_i \times 100 \quad \text{Eq. 2}$$

Additionally, specimens were given a visual rating at the end of exposure to express its condition using the pictorial visual ratings introduced by Bassuoni and Rahman [7].

Thermal and microstructural analyses were performed to investigate the deterioration mechanisms due to the exposure. Differential scanning calorimetry (DSC) was used on powder samples passing through sieve #200 (75 μm) which were prepared by pulverizing fracture pieces extracted from the reaction front (0-10 mm). Microanalysis by scanning electron microscopy (SEM) equipped with energy-dispersive X-ray analysis (EDX) was performed on carbon-coated fracture pieces to support the findings of DSC.

4. Results

4.1. Absorption and Desorption

Table 3 lists the absorption and desorption percentages for each matrix (a mixture with/without a coating). The uncoated samples experienced the highest values for absorption (+6.80, +7.20, and +8.00 for GU, FA, and SG, respectively) and desorption (-3.16, -3.35, and +3.86 for GU, FA, and SG, respectively). Although applying the coatings enhanced the transport properties (lower intake and evaporation rates), dissimilar results were observed. ES yielded superior improvements with average reductions of 80% and 79% for absorption and desorption, respectively. HMMA had moderate improvement with an average absorption of +5.83% and an average desorption of -2.62% for the three mixtures.

Table 3. Absorption and desorption of specimens.

Specimen	Absorption* (+%)						Desorption* (-%)					
	GU		FA		SG		GU		FA		SG	
Uncoated	6.80	[0.52]	7.20	[0.61]	8.00	[0.68]	3.16	[0.16]	3.35	[0.19]	3.86	[0.22]
ES	0.87	[0.08]	1.45	[0.15]	1.93	[0.26]	0.45	[0.03]	0.75	[0.06]	0.94	[0.10]
HMMA	5.20	[0.46]	5.80	[0.51]	6.50	[0.58]	2.40	[0.10]	2.55	[0.12]	2.93	[0.15]

Note: Values between brackets are standard deviations.

4.2. Visual Assessment

Figure 1 shows the final conditions of uncoated and coated specimens along with their visual rating. Uncoated specimens from all mixtures experienced rapid salt depositions onto the drying portion within the first 15 cycles while the immersed portion remained intact (**Figure 2**). Afterwards, salt efflorescence significantly accumulated on the surface followed by the initiation of surface scaling and flaking. After 30 cycles, the rate of surface scaling escalated due to the higher rate of solution supply within and evaporation through concrete until failure of some specimens (SG). Specimens treated with ES showed superior performance compared to uncoated specimens with slight scaling occurred for the GU base mixture, followed by FA and SG, respectively. Comparatively, the HMMA coated layer started to detach after 15 cycles (**Figure 3**) and the coating failed to protect concrete against PSA since all specimens experienced severe surface scaling and/or reduction in cross-sections.



Figure 1. Uncoated and coated specimens at the end of PSA exposure.
(Note: numbers between brackets are the final visual ratings)



Figure 2. Salt efflorescence in the dry portion during exposure.

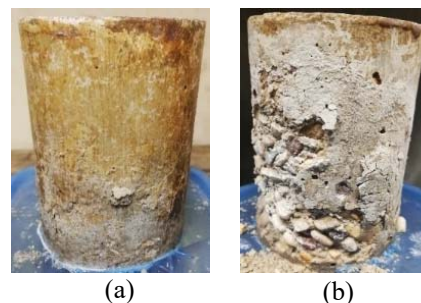


Figure 3. HMMA detachment from the GU specimens after: (a) 15, and (b) 45 cycles.

4.3. Mass Loss

Figure 4 shows the mass loss of uncoated and coated specimens, measured every 30 cycles during the exposure. Uncoated GU, FA and SG specimens had high cumulative mass losses of 12%, 16% and 20%, respectively, indicating the negative effect of large dosages of supplementary cementitious materials. ES application yielded the least values of mass loss with a maximum of 3% for SG-ES specimens, indicating considerable enhancement relative to the reference specimens.

HMMA led to moderate improvement (i.e., average of 20% reduction) in mass loss, compared to that of uncoated specimens with final values of 9%, 13%, and 17% for GU-HM, FA-HM, and SG-HM, respectively.

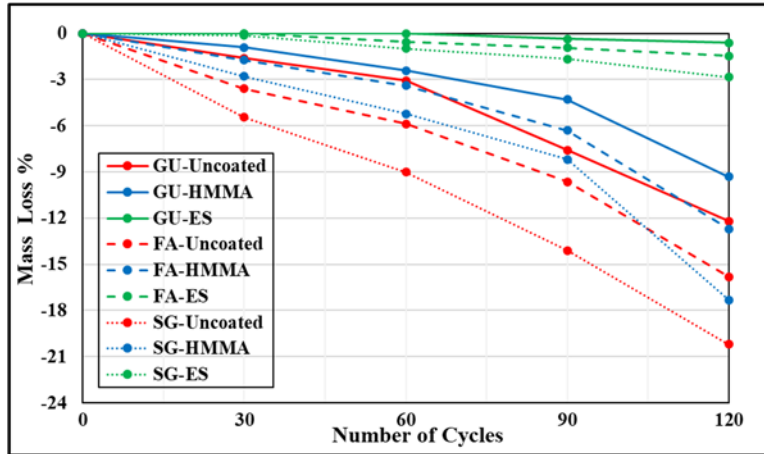


Figure 4. Average mass loss of uncoated and coated specimens throughout the PSA exposure.

5. Discussion

5.1. Damage Mechanism

The damage mechanism is indicated for uncoated concrete since these specimens experienced the highest deterioration levels. The high penetrability of the 0.6 w/b concrete (porosity of 19.5%, 21.8% and 22.5%, respectively for the GU, FA and SG mixtures as determined by the mercury intrusion porosimetry) resulted in rapid rates of capillary rise and solution uptake [7]. This led to the crystallization of high amounts of salt within the surface pores, as determined by the evaporation conditions stimulated by the testing environment. Microanalysis (e.g., **Figure 5**) on the detached surface layer showed the formation of massive amounts of sodium sulfate crystals beneath the surface (sub-efflorescence), which caused the development of significant pressure against the surface layer causing its detachment. SEM images were augmented with DSC analysis on powder sample prepared from extracted pieces from the reaction front (**Figure 6**). The DSC analysis was based on the enthalpy concept (integration of heat flow peaks over temperature) as a semi-quantitative analysis technique to determine the relative phase formation as the enthalpy of each phase is directly related to its quantity [18]. Results showed the limited presence of sulfate reaction products (e.g., ettringite and gypsum) in the drying portion, confirming the physical nature of this damage. Comparatively, the upper portion of specimens had significant amounts of sodium sulfate crystals with the lowest enthalpy occurring for GU (36.65 J/g), followed by FA (39.78 J/g) and SG (45.49 J/g), respectively. These findings suggest that massive formation of sub-efflorescence below the surface layer was the primary cause of damage.

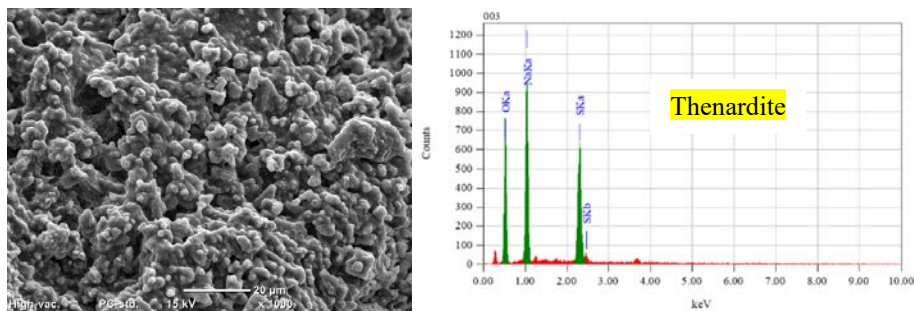


Figure 5. SEM and EDX of the scaled surface layer from uncoated GU specimens after the exposure.

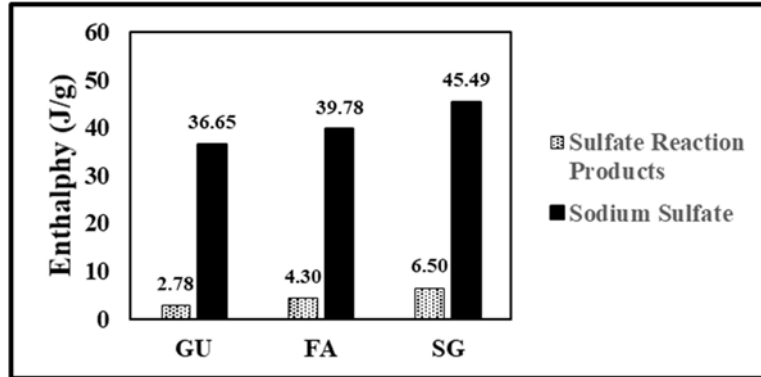


Figure 6. DSC results of uncoated exposed specimens.

5.2. Effect of Supplementary Cementitious Materials

Using high contents of fly ash (40%) and slag (60%) in the binder resulted in inferior performance compared to plain concrete (30% and 65% higher mass losses for the FA and SG specimens, respectively). SEM images for unexposed FA and SG specimens showed notable proportion of unreacted particles within the cementitious matrices [Figure 7 (b) and (c)], with a less compact microstructure compared to that of the GU [Figure 7 (a)]. Unreacted FA and SG particles readily detach as the cyclic exposure proceeded causing higher mass losses compared to the GU concrete, with FA performing better than SG. These dosages of fly ash and slag increased the penetrability of concrete as indicated by the results of absorption/desorption tests (absorption percentages of +6.80, +7.20, and +8.00 for GU, FA, and SG, respectively, and desorption percentages of -3.16, -3.35, and +3.86 for GU, FA, and SG, respectively), conforming to the porosity results.

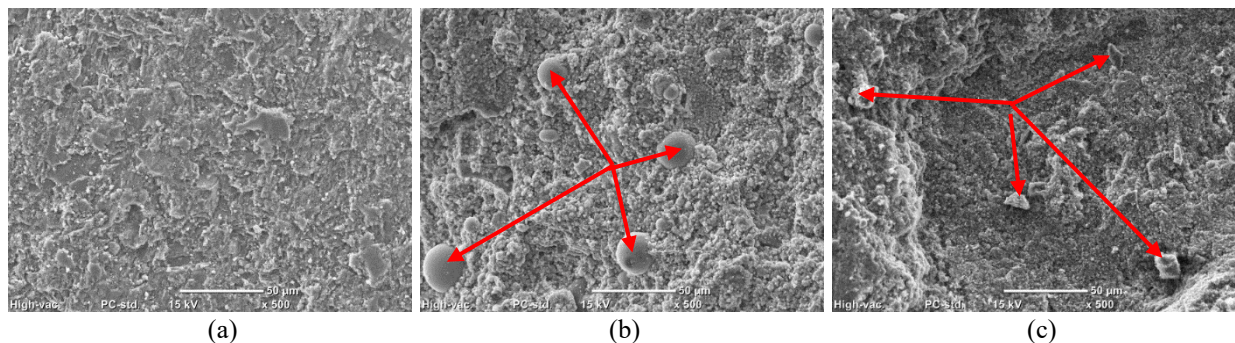


Figure 7. SEM images of unexposed specimens: (a) GU, (b) FA, and (c) SG.

5.3. Protection Mechanisms

Results showed superior performance of all specimens coated with ES, compared to HMMA coated or uncoated specimens. This improvement can be attributed to the dual functionality of ES (water-repelling and pore-blocking). Due to its small particle size, ES easily penetrates into the pores of cementitious matrix and reacts with the hydration compounds, producing hydrophobic agents in addition to calcium silicate hydrate that fills the pores [12], leading to a denser microstructure as shown in Figure 8 (a). This densification of the surface layer considerably decreased the absorption and desorption values of concrete (absorption percentages of +0.87, +1.45, and +1.93 for GU, FA, and SG, respectively, and desorption percentages of -0.45, -0.75, and -0.94 for GU, FA, and SG, respectively), indicating less rates of solution supply and evaporation hence improving the resistance of concrete to wicking and consequently PSA. Accordingly, Figure 9 (a) shows the formation of sodium sulfate traces (small amounts) within the surface layer.

HMMA, based on high-viscosity methacrylate acid, is a crack filler and surface coating agent; it blocks the surface pores and then forms a thin membrane layer on the surface of concrete. Microanalysis showed that after hardening, micro-cracks formed within the coating texture [Figure 8 (b)], which compromised its functionality in resisting wicking of the solution

through concrete. With the progression of the PSA exposure, the HMMA coating was detached from the surface leading to continual surface scaling of concrete at rapid rates similar to uncoated concrete. Accordingly, **Figure 9 (b)** shows that significant amounts of sodium sulfate below the surface layer were the major cause of damage.

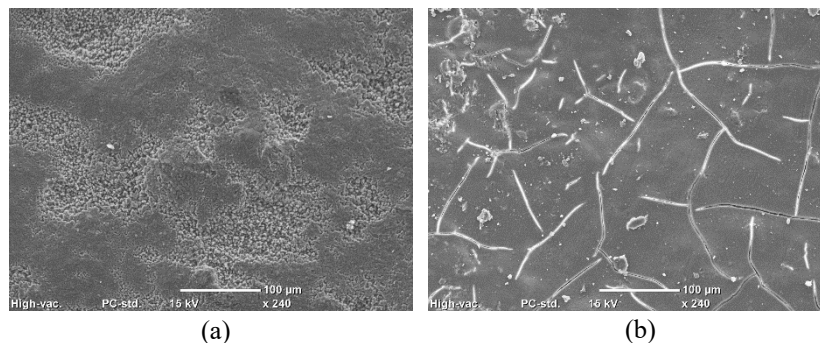


Figure 8. SEM of coated GU concrete surface with: (a) ES, and (b) HMMA before exposure.

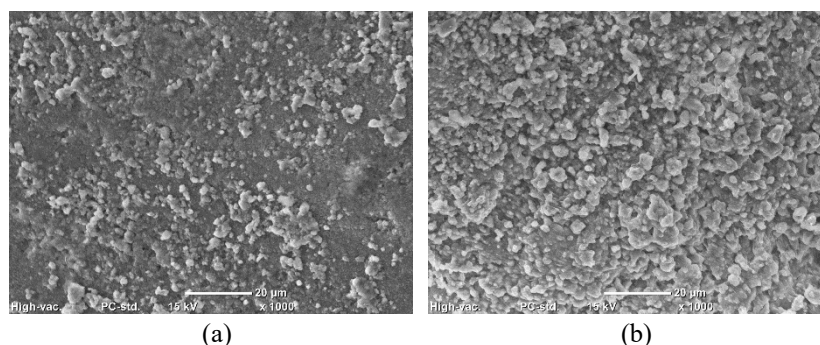


Figure 9. SEM of coated GU specimens with: (a) ES, and (b) HMMA after the exposure.

6. Conclusions

In this study, two polymeric surface coatings commonly used for protection of concrete infrastructure were applied on three concrete mixtures (single and binary blended binders) and tested for their functionality/effectiveness against PSA. Based on the obtained results, the following conclusions can be made:

- Concrete mixtures prepared with high water/binder ratio (0.6), typical of residential concrete, were extremely vulnerable to PSA conditions.
- The use of high replacement ratios of supplementary cementitious materials (40% Fly ash and 60% slag), even with the extended curing period, led to reduced degree of maturity of hydrated paste with high amounts of unreacted particles, and consequently higher vulnerability to PSA.
- HMMA (membrane effect) failed to protect concrete from the aggravated PSA conditions making it unsuitable for field applications.
- The hydrophobic and pore-blocking actions of ethyl silicate were remarkably effective at protecting high porosity concrete from PSA, with promising potential for field applications.

Acknowledgments

The authors highly appreciate the financial support from Natural Sciences and Engineering Research Council of Canada. The IKO Construction Materials Testing Facility at the University of Manitoba in which these experiments were conducted has been instrumental to this research.

References

- [1] ACI Committee 201, "Guide to Durable Concrete (ACI 201.2R-16)," American Concrete Institute, Farmington Hills, MI, 2016, 84 pp.
- [2] Flatt, R. J., "Salt Damage in Porous Materials: How High Supersaturations are Generated," *Journal of Crystal Growth*, V. 242, No. 3-4, 2002, pp. 435-454.
- [3] Haynes, H., and Bassuoni, M. T., "Physical Salt Attack on Concrete," *Concrete International*, V. 33, No. 11, Nov. 2011, pp. 38-42.
- [4] Scherer, G. W., "Stress from Crystallization of Salt," *Cement and Concrete Research*, V. 34, No. 9, 2004, pp. 1613-1624.
- [5] Stark, D., "Durability of Concrete in Sulfate-Rich Soils (RD O97)," Portland Cement Association, Skokie, IL, 1989, 14 pp.
- [6] Stark, D., "Performance of Concrete in Sulfate Environments," R&D Bulletin RD129, Portland Cement Association, Skokie, IL, 2002, 23 pp.
- [7] Sakr, M. R., and M. T. Bassuoni. "Modeling of Parameters Affecting Physical Salt Attack of Concrete." *ACI Materials Journal*, vol. 118, no. 2, 2021, pp. 173-88.
- [8] Bassuoni, M. T., and Rahman, M. M., "Response of Concrete to Accelerated Physical Salt Attack Exposure," *Cement and Concrete Research*, V. 79, 2016, pp. 395-408.
- [9] Zhutovsky, S., and Hooton, R. D., "Experimental Study on Physical Sulfate Salt Attack," *Materials and Structures*, V. 50, 2017, 10 pp.
- [10] Sakr, M. R., Bassuoni, M. T., and Taha, M. R., "Effect of Coatings on Concrete Resistance to Physical Salt Attack," *ACI Materials Journal*, V. 11, No. 6, 2019, pp. 255-267.
- [11] Suleiman, A. R., Soliman, A. M., and Nehdi, M. L., "Effect of Surface Treatment on Durability of Concrete Exposed to Physical Sulfate Attack," *Construction and Building Materials*, V. 73, 2014, pp.
- [12] Barberena-Fernández, A. M., Carmona-Quiroga, P. M., and Blanco-Varela, M. T., "Interaction of TEOS with Cementitious Materials: Chemical and Physical Effects." *Cement and Concrete Composites*, vol. 55, 2015, pp. 145-52.
- [13] Rahim, A., Jansen, D., Abo-Shadi, N., and Simek, J., "Overview of High-Molecular-Weight Methacrylate for Sealing Cracks in Concrete Bridge Decks." *Transportation Research Record*, no. 2202, 2010, pp. 77-81.
- [14] CAN/CSA-A3001, "Cementitious Materials for Use in Concrete," Canadian Standards Association, Mississauga, ON, Canada, 2013, 691 pp.
- [15] ASTM C39/C39M-12, "Standard Test Method for Compressive Strength of Cylindrical Concrete Specimens," ASTM International, West Conshohocken, PA, 2012, 7 pp.
- [16] ASTM C192/C192M-12, "Standard Practice for Making and Curing Concrete Test Specimens in the Laboratory," ASTM International, West Conshohocken, PA, 2012, 8 pp.
- [17] CSA A23.1/A23.2, "Concrete Materials and Methods of Concrete Construction/Test Methods and Standard Practices for Concrete," Canadian Standards Association, Mississauga, ON, Canada, 2019, 882 pp
- [18] Novák, Csaba. "Handbook of Thermal Analysis and Calorimetry, Series Editor: Patrcik K. Gallagher, Volume 1, Principles and Practice, Editor: Michael E. Brown, Elsevier 1998, ISBN 0 444 82085 X." *Journal of Thermal Analysis and Calorimetry*, vol. 57, no. 2, Kluwer Academic Publishers, 1999, pp. 623-24.